The effect of pore microstructure on strength and chloride ingress in blended cement based on low kaolin clay

Ram, Kiran; Serdar, Marijana; Londono-Zulua, Diana; Scrivener, Karen

The effect of pore microstructure on strength and chloride ingress in blended cement based on low kaolin clay

Article *in* Case Studies in Construction Materials · June 2022

DOI: 10.1016/j.cscm.2022.e01242

CITATIONS
15

READS
179

4 authors, including:

Kiran Ram
Mott MacDonald Group
15 PUBLICATIONS **38** CITATIONS
SEE PROFILE

Marijana Serdar
University of Zagreb
131 PUBLICATIONS **1,415** CITATIONS
SEE PROFILE

Diana Londono-Zuluaga
Cementir Holding
33 PUBLICATIONS **484** CITATIONS
SEE PROFILE

Case Studies in Construction Materials 17 (2022) e01242

Contents lists available at ScienceDirect

Case Studies in Construction Materials

journal homepage: www.elsevier.com/locate/cscm

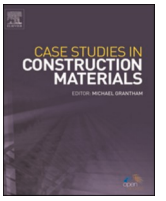

Case study

The effect of pore microstructure on strength and chloride ingress in blended cement based on low kaolin clay

Kiran Ram [a], Marijana Serdar [a,*], Diana Londono-Zuluaga [b], Karen Scrivener [b]

[a] Department of Materials, Faculty of Civil Engineering, University of Zagreb, 10000 Zagreb, Croatia
[b] Laboratory of Construction Materials, École Polytechnique Fédérale de Lausanne, 1015 Lausanne, Switzerland

ARTICLE INFO

Keywords:
Limestone calcined clay cement
MIP
Surface resistivity
Sorptivity indices
Chloride migration coefficient
Chloride diffusion coefficient

ABSTRACT

The objective of this study is to analyse the mechanical and durability properties of a high-performance mortars based on low grade kaolin clay and the effect of electrical conductivity and pore microstructure on the chloride penetration resistance. A total of six mixes were prepared with binary and ternary binders in which a high volume of cement was replaced by low-grade calcined kaolin clay, fly ash and limestone powder. The percentage of kaolinite in the clay used from the Southeast European region was less than 20%. The variations in compressive strength and chloride transport coefficient were analysed experimentally and related to the pore structure and electrical conductivity. Compressive strength, chloride migration and diffusion coefficients, and bulk conductivity were determined using mortar samples, while the pore size distribution was determined by mercury intrusion porosimetry (MIP) on hardened cement paste after 7,28, and 90 days of curing. To understand the capillary absorption of these mixtures, sorptivity indices were measured after 28 and 90 days. The experimental characteristics of the pore size distribution, such as mean pore entry radius ($r_{0.5}$), permeable porosity (P), capillary porosity (ϕ), and critical pore diameter (r_c), were calculated using the cumulative data of the intruded volume as a function of pressure obtained by MIP. In addition, the extrusion-intrusion curve was used to calculate the pore entrapment fraction (α) and the degree of interconnectivity of the pore structure. The evolution of pore structure parameters was monitored for up to 90 days and their effects on strength and chloride penetration were studied in detail. The results showed that all mixes (even those with low kaolinite content) can be used in high performance cement systems and the pore structure has a limited effect on chloride penetration.

1. Introduction

In recent decades, cement industry researchers have concentrated on developing suitable cement additives (SCMs) to mitigate CO_2 emissions associated with cement manufacture. The industry's aim is to manufacture blended cements with the lowest possible CO_2 emissions without sacrificing critical concrete characteristics like as strength and durability. Recent studies have demonstrated that the cement industry cannot continue to rely on conventional SCMs such as siliceous fly ash and blast furnace slag in the long run due to their source depletion [1]. Therefore, there is a need for alternatives that meet both quantitative and qualitative requirements for

* Corresponding author.
E-mail addresses: kiran.ram@grad.unizg.hr (K. Ram), marijana.serdar@grad.unizg.hr (M. Serdar), diana.londonozuluaga@epfl.ch (D. Londono-Zuluaga), karen.scrivener@epfl.ch (K. Scrivener).

https://doi.org/10.1016/j.cscm.2022.e01242
Received 18 February 2022; Received in revised form 5 June 2022; Accepted 10 June 2022
Available online 15 June 2022

construction materials. Calcined clays, especially in combination with limestone, could be a promising alternative combination to reduce the environmental footprint of cement [2]. Due to better synergetic action between clays, limestone and clinker, the higher level of replacement can be achieved in the so-called LC3 systems (limestone-calcined clay cement) [3]. The primary raw material for LC3 production, in addition to clinker, is clay, which is abundantly available all over the world. The presence of kaolinite in clays has been found all over the world, but the amount of kaolinite present varies from one region to another, and this is a critical factor in their overall performance. Clays containing a significant proportion of kaolinite have been shown to be highly pozzolanic when calcined between 700℃ and 850℃ [4]. The hydration kinetics of limestone-calcined clay cement were indeed significantly influenced by the kaolinite content, which affects the mechanical and chloride transport properties of the concrete [5,6]. However, high grade kaolin clays are not easily available everywhere or they have a more favorable application. One of the possibilities to consider is using low grade kaolin clays, more easily available in sufficient quantities for cement industry. Notwithstanding, recent developments in LC3-based concrete have shown that an intermediate level of kaolin clay may be an appealing option, particularly given its widespread availability [7,8].

According to previous research, concrete containing SCMs has a higher resistance to chloride penetration, which is primarily due to the improved pore structure[8,9]. Halamickova et al., reported that the chloride diffusion coefficient varies linearly with critical pore entry radius as determined by the Mercury Intrusion Porosimetry (MIP) technique [10]. Although the MIP approach has several drawbacks, it is still a useful tool. One of the major drawbacks of commercial porosimeters is that mercury does not penetrate the very fine pores, which range in size from 1 nanometer to 3 nanometers [11]. In addition, the "ink-bottle" impact and the gel's segmentation of capillary pores can result in an overestimation of fine pores and an underestimation of larger capillary pores [11,12]. Nevertheless, the porosity obtained by MIP is a permeable porosity that covers most of the interconnected pores that have a direct impact on the durability of concrete [13]. The intrusion-extrusion cycle in MIP can also indicate the presence of entrapped pores, which is expressed as a network of discontinuous pores [14], which is expressed as network of discontinued pores. Understanding the porosity and pore size distribution of cement-based materials with various SCMs can be used to endorse chloride penetration. However, Shiyu et al. found that the electroneutrality of the pore solution and the surface properties of the hydration product influence the chloride transport in ternary blended cementitious systems more than their pore structure [15]. Additionally, electrical resistivity had an impact on chloride transport in cementitious systems, particularly when it came to the movement of chloride by electrical potential [16–20]. The approach fully excludes the impacts of other negatively charged species in the pore solution, making it the most disadvantageous of the electrically accelerated processes[21].

The primary goal of this study is to determine the endurance of a cementitious system composed primarily of low-grade kaolin clay in harsh coastal conditions. A low-grade kaolin clay (containing 20% kaolinite) and limestone were combined to produce a mortar with a high cement substitution level. The chloride penetration resistance and compressive strength of this mortar were compared to those of mortars with a similar degree of cement substitution by fly ash and limestone, as well as to those of reference mortars based on pure clinker cement (CEM I) and blended cement with slag (CEM III/B). Furthermore, this study attempted to demonstrate how pore structure parameters affect compressive strength and chloride penetration. Also, the influence of conductivity on chloride penetration and movement in blended mixes is discussed. The mechanical properties and durability of each mix were found to be related to the pore structure, while the chloride transport coefficients were found to be related to the bulk conductivity and surface resistivity. The findings of this study contribute to a better understanding of the effect of pore structure on chloride transport, particularly in low-grade limestone-calcined clay cements.

2. Materials and methods

2.1. Binder composition

Six mixes were prepared for this study, where Portland cement (CEM I 42,5 R) was used as the primary binder. Binary binder systems were prepared with 70% CEM I and 30% SCM, with mixes labeled FA30 (mix with 30% fly ash) and CC30 (mix with 30% calcined clay). Ternary binder systems were prepared with 70% CEM I, 30% SCM and 15% limestone, with mixes labeled FA30LS15

Table 1
Chemical composition and particle size distribution of materials used in the study.

Component	CEM I	CEM III	Fly ash (FA)	Calcined clay (CC)	Limestone (LS)
CaO	63.19	31.28	11.52	1.74	71.59
SiO_2	19.51	38.83	53.28	49.80	20.21
Al_2O_3	4.21	10.34	19.11	17.04	4.32
Fe_2O_3	2.85	1.32	9.05	5.80	1.43
MgO	0.85	9.73	2.78	1.42	1.69
Na_2O	0.20	0.87	0.26	0.84	0
K_2O	0.48	1.82	1.51	2.00	0.15
TiO_2	0.12	0.31	0.52	0.75	0.52
P_2O_5	0.45	1.55	0.36	0.29	0.42
SO_3	2.3	0.01	1.48	0.06	1.48
D_{10}, μm	0.32	0.45	1.55	4.03	3.43
D_{50}, μm	9.95	12.71	15.24	10.72	18
D_{90}, μm	50	58.85	72.68	24.79	63.82

(mix with 30% fly ash and 15% limestone) and CC30LS15 (mix with 30% calcined clay and 15% limestone). Additional to these mixes, CEM III/B (36–65% replaced with slag) was also used to compare the properties of blended binder systems with commercially available binders. Tables 1 and 2 show the chemical composition of each constituent and mineralogical components of SCMs respectively. More information about these materials, such as reactivity obtained using isothermal calorimetry and bound water test can be found in previous paper [22]. Fig. 1 illustrates Scanning Electron Microscopy (SEM) images of fly ash and clay to understand the surface morphology of the materials and Fig. 2 shows the particle size distribution of used materials. The kaolinite content of calcined clay was 17% by thermogravimetric analysis [23]. All SCMs were previously dried at 60 ℃ for 24 h and ground in disc mill for 30 s. In the case of calcined clay, the dried ground raw clay was calcined in a furnace at 800 ± 20 °C for one hour and preparation of clay followed by the protocol [24]. All mortar mixtures were prepared using crushed sand (0–4 mm) and water-binder ratio of 0.5.

The mortar mix was prepared and fresh state properties (flow, temperature, density and air content) tested in accordance with EN 196–1 [25]. The mortar specimens were cast in a prismatic mould (40 × 40 × 160 mm) for tensile and compressive strength testing, and a cylindrical specimen with a diameter of 100 mm and a height of 200 mm was prepared for chloride migration and diffusion test. Cylindrical specimen with a diameter of 70 mm and height of 100 mm were prepared for sorptivity indices and water-filled porosity test. After 2, 7, 28, and 90 days of curing, compressive strength tests were performed, and chloride tests were performed after 7, 28, and 90 days of curing. Sorptivity test was performed after 28 and 90 days of curing. All specimens were kept in a moisture-controlled room for curing until the specified time of testing. Three specimens were taken for compressive strength, chloride transport coefficients, bulk conductivity, surface resistivity, and sorptivity and pore structure determined on mortar samples.

2.2. Chloride transport coefficients

The resistance to chloride penetration was evaluated by both migration and diffusion experiments according to standards NT BUILD 492 [26] and NT BUILD 443 [27], respectively. In both tests, the cylindrical specimens were cut into three specimens with thickness of 50 mm. All the specimens were preconditioned by saturated Ca $(OH)_2$ solution in vacuum for 24 h. Following the procedure described in standard NT BUILD 492, the non-steady state migration coefficients were calculated based on measured chloride penetration depth under forced movement (by external potential) of chloride ions across the mortar specimen. In this method, a quick qualitative assessment regarding chloride ingress resistance can be obtained. In migration test, after exposure to prescribed external potential, specimens were cut diametrically after the test duration and sprayed with the silver nitrate solution to measure the depth of penetrated chlorides. The equation used to calculate the non-steady state chloride migration (D_{nssm}) coefficient is given below:

$$D_{nssm} = \frac{RT}{zFE}\cdot\frac{x_d - \alpha\sqrt{x_d}}{t} \quad (1)$$

where x_d is the average measured depth of chloride penetration after the test duration, while other parameters were taken from the NT BUILD 492.

In the diffusion test, the specimens were coated with epoxy resin on all sides except the bottom one for chloride exposure. After coating, the specimens were left another 24 h for epoxy to fully dry, and then fully immersed in 16.5% NaCl solution for 35 days. After 35 days, the profile grinding (depths were taken according to NT BUILD 443) was performed to obtain powder for chemical analysis. The total chloride content in the powder was determined using potentiometric titration method described in standard EN 14629–2007 [28]. Thereafter, the effective chloride diffusion coefficients (D_E) were determined by fitting the total chloride contents in second Fick's law according to NT BUILD 443:

$$C\quad(x,t) = C_s - (C_s - C_i).\mathrm{erf}\left(x\middle|\sqrt{4D_E t}\right) \quad (2)$$

where C(x,t) is the measure chloride content at depth (x) and exposure time (t). The values of apparent chloride diffusion coefficients could be extracted after fitting the measured chloride contents. Additionally, the relation between non-steady state chloride migration coefficient and effective diffusion coefficients were determined.

Table 2
Mineralogical data of clay and fly ash used in this study.

Component	Fly ash (FA)	Calcined clay (CC)
Quartz	5.4	21.7
Muscovite	–	27.3
Mullite	2.2	–
Vermiculite	–	2.4
Illite	–	1.3
Hematite	0.3	–
Amorphous content	89.3	14.3
Loss of Ignition (%)	8.22	7.60

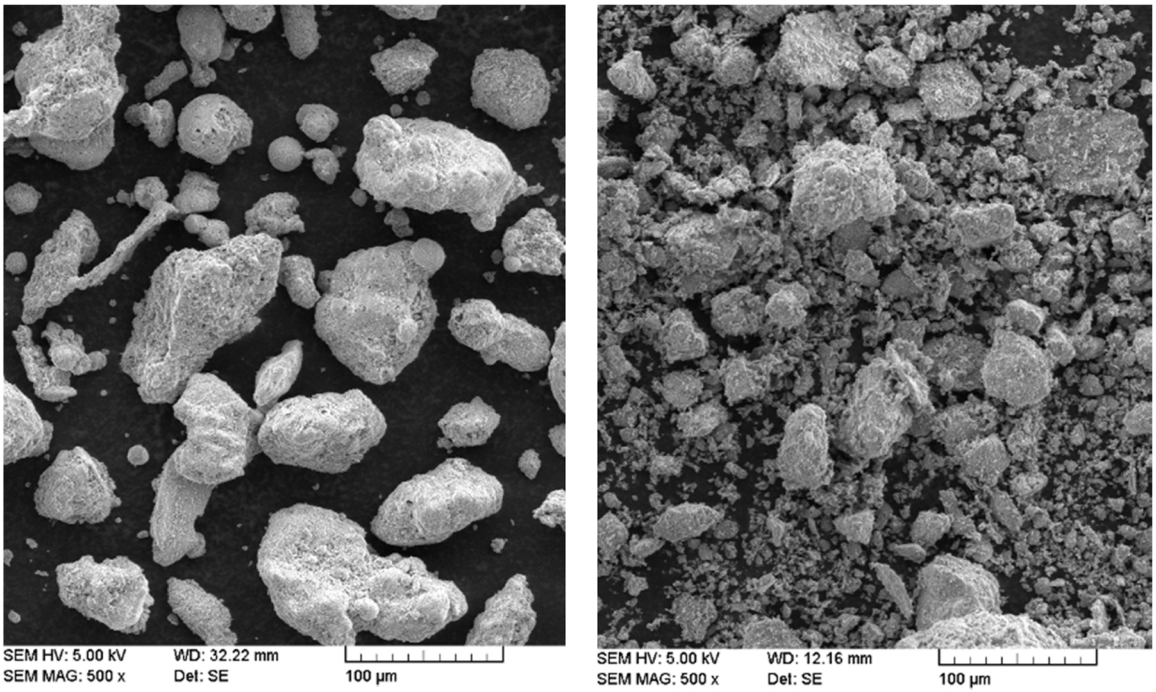

Fig. 1. SEM images of fly ash (left) and calcined clay (right).

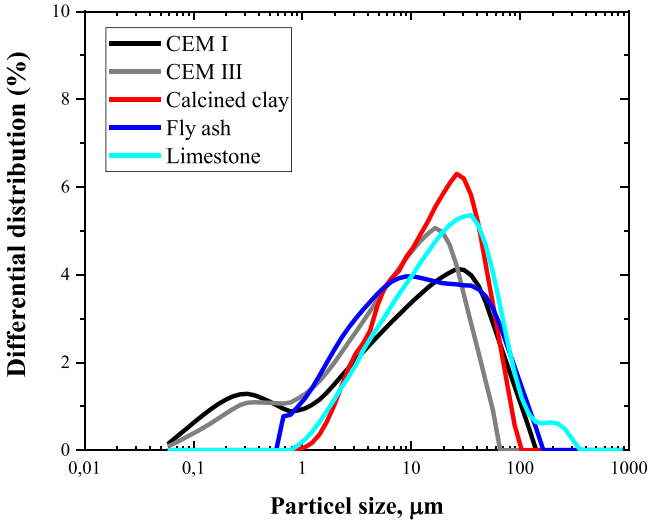

Fig. 2. Particle-size distribution of various materials used in the study.

2.3. Bulk conductivity and surface resistivity

The initial current values from chloride migration experiment were used to calculate the bulk conductivity of the specimen according to ASTM C 1760 [29] according to the following Equation:

$$Conductivity, \quad \sigma = 1273.2 \quad .\frac{I_i}{V}.\frac{L}{D^2} \tag{3}$$

where 'I_i is measured as initial current by imposing voltage of 'V' to the specimen and other parameters were taken from the standard. The bulk resistivity of the pore solution was calculated as the reciprocal of the conductivity obtained from Eq. (3).

The surface resistivity of each mixture was determined by Wenner 4-probe resistivity meter on the sides of cylindrical specimens,

which was used to determine the chloride transport coefficients [30]. The measurements were taken in saturated condition at four different locations of each specimen. A total of 12 readings were taken and the average reported as surface resistivity.

2.4. Sorptivity and water-filled porosity

The sorptivity and water-permeable porosity of each sample was determined based on South African Durability Index Manual [31]. After the curing, the specimen was dried at 50℃ for 7 days and then stored for 4 h in a desiccator. Specimens were placed on the tray, which contains saturated Ca $(OH)_2$ solution. Specimens were supported by wooden rollers and the level of solution was limited to 2 mm from the surface. The weight of specimen was noted down after 3, 5, 9, 12, 16, 20, and 25 min. After the weight estimation, the samples were conditioned in saturated calcium hydroxide solution for one day. The calculation of sorptivity index was performed using Eq. (4).

$$S = \frac{F \quad \times d}{M_{sv} - M_{S0}} \tag{4}$$

where 'F' is the slope of the best fit line between mass gain and square root of time, average thickness 'd', M_{sv} and M_{S0} are the vacuum weight and initial weight of samples. The water-permeable porosity (P) can be calculated using Eq. (5).

$$P = \frac{M_{sv} - M_{s0}}{A \quad \times d \times \quad \rho_w} \tag{5}$$

2.5. Pore structure parameters using mercury intrusion porosimeter (MIP)

Mercury intrusion porosimetry (MIP) with up to 400 MPa was used to measure the pore structure parameters for each mix. The pore entry radiuses were calculated by combining the results from Pascal 140 and Pascal 440 instruments, assuming a contact angle of mercury as 140^0. For MIP, cement paste specimen with the same mixture composition was prepared and cured in humidity chamber for the desired curing periods. After curing, the hydration was stopped using solvent exchange method with isopropanol immersion for 7 days. Subsequently, the samples were dried under vacuum for 48 h. During the MIP test, the pressures were transferred to the pore entry diameter using Washburn equation[32]. The hardened properties of cement based systems mostly depend on the volume of capillary pores, i.e. pores in the range of diameter between 10 nm and 10 μm [33]. The critical pore entry radius (r_c) represents the grouping of the largest fraction of interconnected pores in cementitious system. Critical pore entry radius is corresponding to the peak in the differential pore volume curve indicating the pore size corresponding to the maximum volume intrusion. After the test, total cumulative and differential curves were obtained for each sample. Capillary pore volume (ϕ) of a mixture was evaluated as the total pore volume in the range of 10–10000 nm pore diameter [35]. The critical pore entry radius (r_c) was determined as the diameter at the maximum value of differential pore volume in distribution curve. Mean pore entry radius ($r_{0.5}$) was evaluated based on the following equation [33],

$$\ln r_{0.5} = \frac{\sum_{i=1}^{n} \ln v_i r_i}{\sum Vi} \tag{6}$$

where, for the continuous intrusion curve divided into n discrete radii ranges, v_i is the incremental intrusion of mercury corresponding to i^{th} radius range represented by the mean radius r_i. Pore entrapment can be determined from the intrusion-extrusion curves of MIP. The pore entrapment fraction α is defined as ratio of the pore entrapment volume and the total intrusion volume, Eq. (6).

$$\alpha = \frac{Pore \quad entrapement \quad volume}{Total \quad intusion \quad pore \quad volume} \tag{7}$$

Pore entrapment fraction explains the complexity of pore structure. Larger pore entrapment indicates the higher complexity in pore structure, and pore distribution with high unevenness [34].

Table 3
Fresh properties of the mixes used in this study.

Mix	Flow diameter, mm	Temperature,^{0}C	Density, kg/m^3	Air content, %
CEM I	169.5	17.4	2353.7	2.6
CEM III	175	17.3	2320	2
FA30	156	19.6	2270	2.7
CC30	165	19.5	2325	2.4
FA30LS15	162.5	18.8	2272	2.4
CC30LS15	150	20.7	2320	2.1

3. Results

3.1. Evolution of mortar compressive strength

All mixtures were made with a water-to-binder ratio of 0.5. Table 3 shows the fresh properties of all mixtures. In their fresh state, mixes have similar consistency, density, and air content. The mixture with limestone-calcined clay has a smaller flow diameter, which is in accordance with the previous studies [35]. In general, fly ash improves cementitious system flow, but in this case, the flow was reduced. Fly ash used in this study has a lower percentage of spherical particles, as can be seen in the SEM images (Fig. 1). Furthermore, the fly ash has a higher loss value of loss of ignition (8.22%). Fly ash used came directly for the industry, material was not pretreated or selected and it consists of a high amount of unburned carbon. The unburned carbon potentially consumed more water from the system and caused the low flowability in this system [36].

After 2, 7, 28, and 90 days of curing, the compressive strength of the mortar mix was evaluated, and the results are shown in Fig. 3. The initial strength of ternary mixes was lower than CEM I mix, which was expected due to the slow reactivity and dilution effect of limestone powder. In the case of calcined clay, lower initial strength was also anticipated since used clay has a relatively low amount of kaolinite, which directly influences the strength development [5]. After 7 days both fly ash and calcined clay mixes improved their strength. The highest increase for CC30 mix was achieved between 7 and 28 days, while FA30 mix gained comparable strength after prolonged (after 90 days) curing.

The pattern of strength gain in the ternary binder system was comparable to that of the binary system, although the final obtained strength was lower. When compared to fly ash mixtures, calcined clay mixes with and without limestone had higher strength after 28 days, but the tendency reversed with longer curing. Finally, even though FA30LS15 and CC30LS15 contain just 55% cement, they reached a compressive strength of 65–70% of that of CEM I mortar after 90 days of curing. Despite the lower clinker percentage, the synergistic effect of limestone and alumina in SCMs is clearly responsible for the comparable performance of ternary mixes [37,38]. CEM III mix showed the lowest strength at all curing ages compared to CEM I and binary mixes, but a comparable compressive strength at all ages of curing to that of ternary mixes. Unlike most fly ash systems, the present one had the same strength as CEM I after 7 days. This was clearly due to the higher lime content of fly ash used [39].

3.2. Evolution of chloride transport coefficients

Chloride diffusion and migration coefficients were determined for better understanding of the chloride transport. The non-steady state chloride migration coefficients of each mix evaluated after 7, 28, and 90 days of curing are presented in Fig. 4. Compared to the CEM I specimen, the addition of fly ash and calcined clay reduced the chloride migration coefficient by 25–30% after 28 days and approximately 30–35% after 90 days in binary binder systems. After 7 days of curing days, ternary blends showed very high values of migration coefficient, which is correlated to their high electrical conductivity at early ages [40]. However, after 28- and 90-days chloride migration coefficients were significantly lowered for CC30LS15 (lowered 56% after 28 days and 83% after 90 days) and FA30LS15 (lowered 54% after 28 days and 80% lowered after 90 days) mixes. Thus, the chloride penetration resistance significantly improved ternary mixes after 90 days, even with very low kaolin clay. CEM III specimen exhibited the highest chloride penetration resistance among all the mixes despite of lower compressive strength.

The effective chloride diffusion coefficients were also determined based on chloride profile, and the results are shown in Figs. 5 and 6. The chloride content of eight layers (0.5 mm from the exposure surface to 22.5 mm) were measured after the mortar specimen thoroughly immersed in sodium chloride solution for 35 days. A total chloride content of each layer was determined to evaluate the chloride diffusion coefficient at different curing ages.

Chloride migration coefficients are much higher than diffusion coefficients at all ages. The higher values of migration might be due to the electrical gradient caused by ions, the interaction between ions and cementitious phases, the dissolution of the cementitious

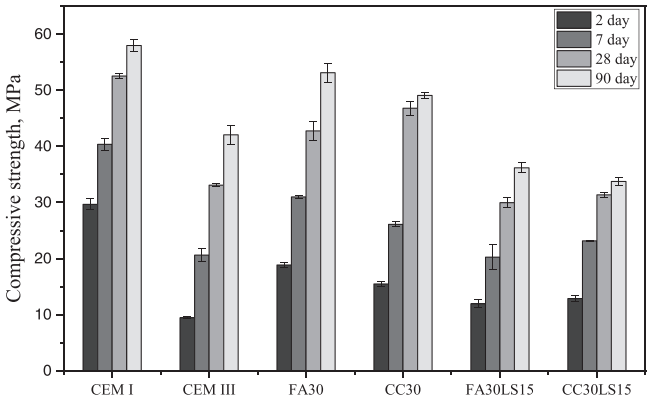

Fig. 3. Evolution compressive strength of all mixes.

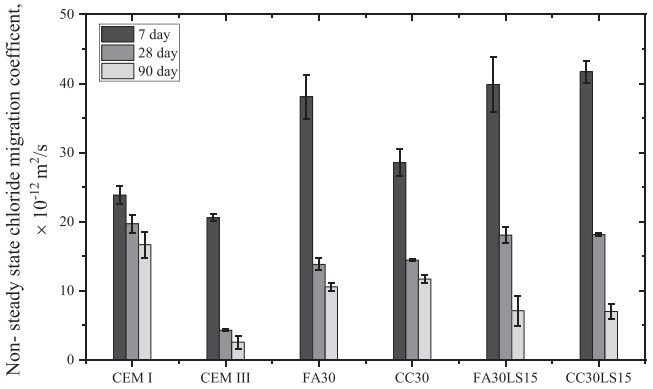

Fig. 4. Evolution of non-steady state chloride migration coefficient of all mixes after 7, 28 and 90 days of curing.

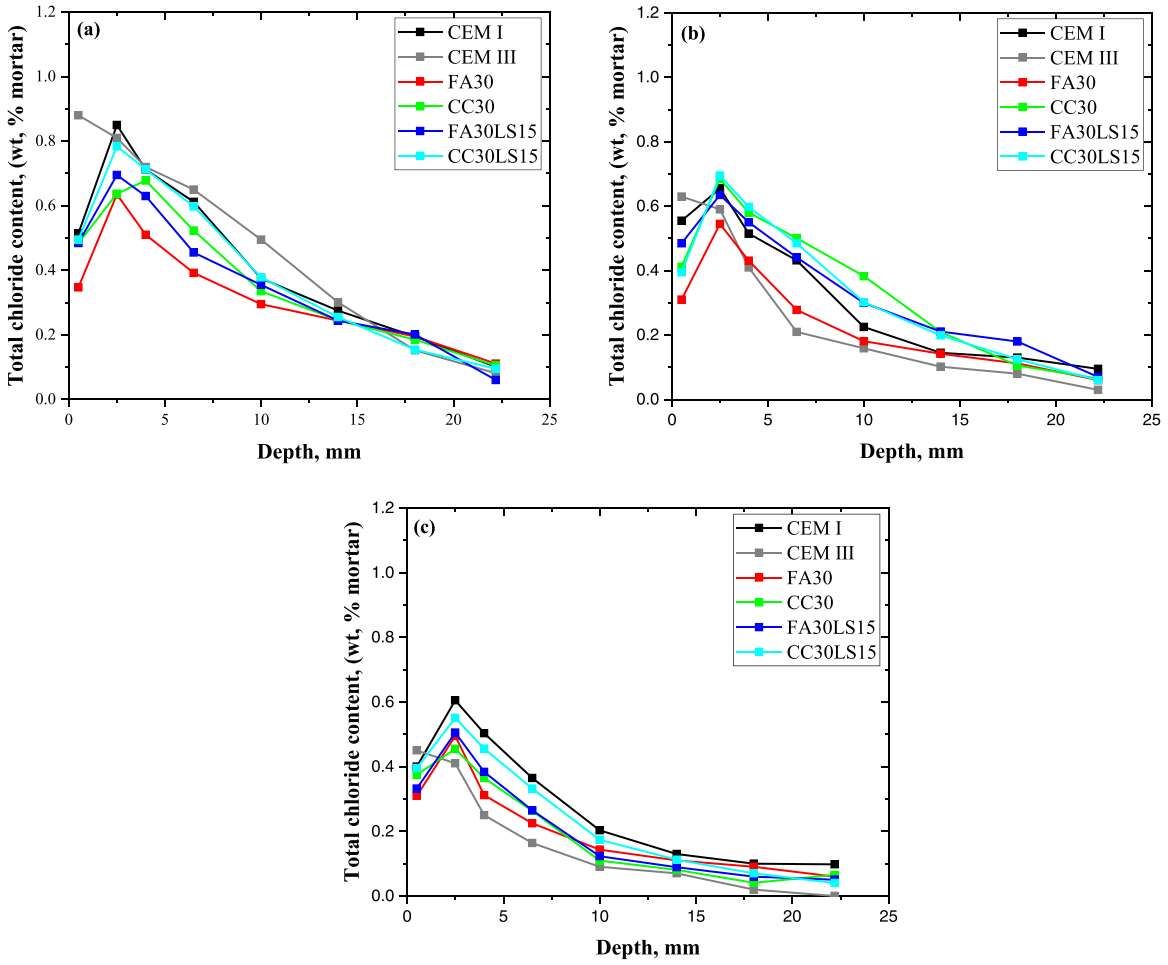

Fig. 5. Chloride profile of different mixes after 7 days (a), 28 days (b), and 90 days (c) in 16.5% NaCl solution.

matrix, chemical deposition on pore walls and combined effect of all these factors [41].

The CEM I mix showed higher rates of chloride ingress compared to all composite mixes at 28 days. This can be attributed to lower porosity and higher ionic resistance of binary and ternary blended mixes [42]. Among the ternary and binary systems, the lowest chloride diffusion coefficient was observed for fly ash mix after prolonged curing. In overall, CEM III specimen showed lowest chloride diffusion coefficient similar to chloride migration.

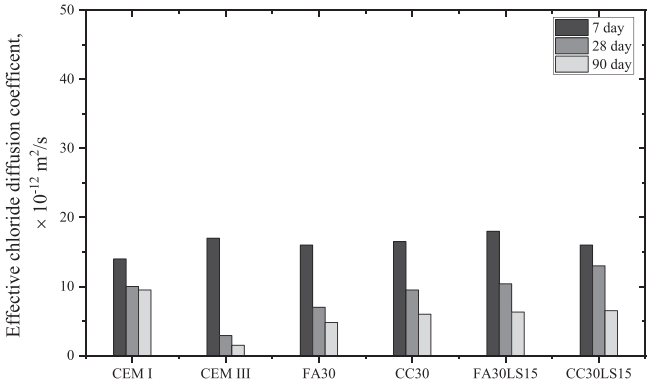

Fig. 6. Effective state diffusion coefficients of all mixes after 7, 28 and 90 days of curing.

3.3. Electrical conductivity and surface resistivity

Fig. 7 shows the conductivity variation of each binder systems at different ages. The trend is clearly attributed to the chloride migration property of each mix. All of the binder systems had high conductivity at 7 days and then decreased as the curing time increased. After 90 days, CEM III has a significant reduction in conductivity (nearly 85%), which is supported by the results of chloride migration.

Fig. 8 depicts the surface resistivity of each mixture measured using Wenner probe. CEM III showed the highest surface resistivity among all mixtures and all blended mixes showed better resistance than CEM I. The surface resistivity reached similar range of values (30–35 k.ohm.cm) for all blended mixtures at 90 days.

3.4. Sorptivity

The absorption rate, which is attributed to the sorptivity index, is commonly used to evaluate the capillary absorption of cementitious systems. The concrete can be classified based on its soprtivity values according to the limiting values proposed by Alexander et al. [43].

Fig. 9 illustrates the sorptivity indices of all the mixtures. After 28 days of curing, the mixtures with calcined clay showed better soprtivity index than other mixes, whereas the ternary blended showed the least absorption tendency after prolonged curing. The addition of fly ash and calcined clay improved the absorption resistance of moisture, especially with combination of limestone powder.

3.5. Evolution of pore structure

Fig. 10 shows the pore size distribution of each specimen after 7, 28, and 90 days of curing, respectively. Table 4 presents calculated pore structure parameters, such as total permeable porosity, mean pore radius ($r_{0.5}$), and critical pore radius for each mix.

The differential intrusion curves illustrate that critical pore size changed with curing time, and that the total pore size range was steadily reduced with prolonged curing. While considering the differential intrusion curve, binary and ternary mixes showed better refinement of pore structure parameters compared to CEM I. The differential curves are getting more narrowed in calcined mixes and thus a finer critical radius was measured compared to other mixes. The capillary pore volume, mean pore entry radius, critical pore

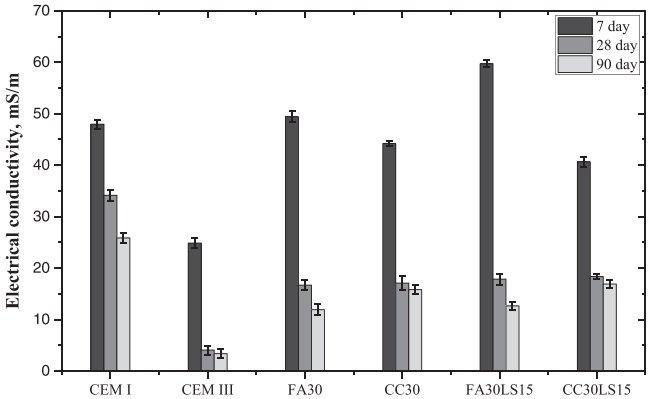

Fig. 7. Evolution of electrical conductivity of all mixes after 7, 28 and 90 days of curing.

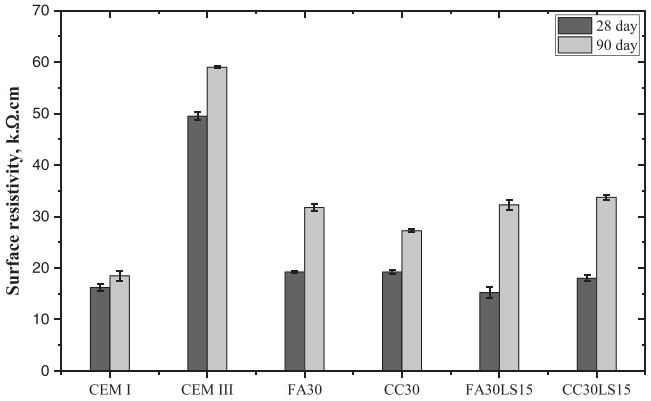

Fig. 8. Surface resistivity of all mixture after 28 and 90 days of curing.

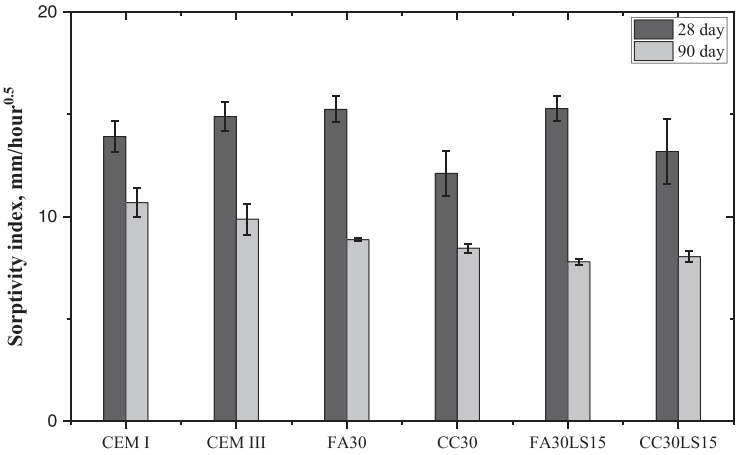

Fig. 9. Sorptivity index of all mixes after 28 and 90 days of curing.

entry radius, and pore entrapment fraction were determined from MIP curves and all the data are given in Table 3. It can be observed that the parameters describing pores were significantly reduced from 7 days to 90 days of curing for all mixes. On the other side, parameters which can be used to describe the absence of inter-connectivity of pores (pore entrapment fraction) increased with prolonged curing.

4. Discussion

In the first part of the discussion, different durability parameters are compared to understand, eliminate, or highlight their impact on chloride diffusion. Among correlations which are analysed are correlation between chloride migration and diffusion coefficients, and the impact of electrical resistivity and sorptivity on these coefficients. In the second part of the discussion, parameters of pore structure are correlated to mechanical and durability properties of tested mortars, to analyse whether the differences in properties of blended systems can be explained by the pore structure.

4.1. Relation between different durability properties

4.1.1. Relation between chloride migration and diffusion

The migration coefficients were much higher than the diffusion coefficients across all tested ages and for all mixes, with similar trend reported in previous studies [44]. Fig. 11 shows the correlation between chloride migration and chloride diffusion for all tested mixes, with a coefficient of determination $R^2 = 0.94$.

$$D_{nssm} = 1.86 \quad \times D_E$$

The migration coefficients and diffusion coefficients for tested mixes are strongly correlated, but with chloride migration values being 1.86 times higher than the values of chloride diffusion. This is especially evident in early ages of blended mortars, where the values of chloride migration coefficients are significantly higher than those of chloride diffusion. The higher values of migration

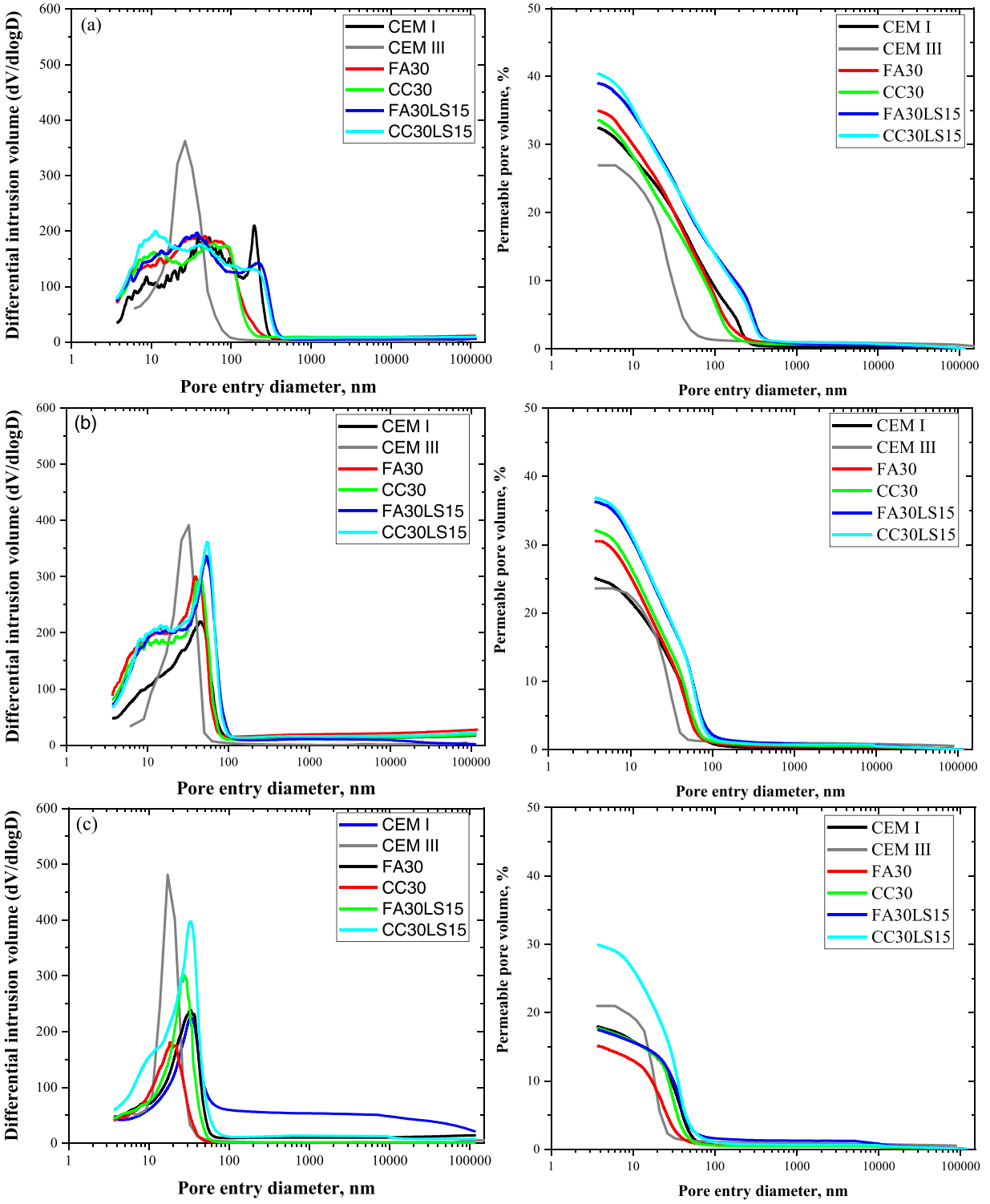

Fig. 10. Differential intrusion curve after a) 7-days, b) 28-days, and c) 90 days curing.

coefficients than diffusion coefficients could be explained by the single species theory assumption in the calculation, which is not taking into the account the effect of other charged ions in the pore solution on chloride penetration [21]. Therefore, despite the obvious advantage of the rapid method for testing chloride migration, the migration coefficients obtained will be an over-estimation of chloride ingress compared to the coefficients obtained by diffusion test. These types of correlation were developed in various studies, and are especially useful to determine the diffusion coefficients and the service life [45]. For instance, the relation between design values of the

Table 4
Pore structure parameters from MIP analysis.

Mix	Age, days	Permeable porosity, %	Median pore entry radius ($r_{0.5}$) nm	Critical pore entry radius (r_c) nm	Capillary pore volume, %	Pore entrapment fraction (α)
CEM I	7	32.5	23.42	23.22	27.8	0.46
	28	25.14	15.93	19.35	20.93	0.54
	90	18.03	15.73	16.535	15.34	0.62
CEM III	7	26.96	10.71	13.37	23.40	0.41
	28	23.59	11.26	12.68	21.12	0.43
	90	20.1	8.48	8.99	18.13	0.68
FA30	7	35.01	19.93	32.54	29.43	0.53
	28	30.49	12.98	19.62	25.01	0.57
	90	15.17	10.63	9.42	12.55	0.74
CC30	7	33.65	18.56	31.19	27.58	0.49
	28	32.1	13.50	22.91	26.34	0.53
	90	15.8	14.30	13.73	12.42	0.73
FA30LS15	7	39.04	25.41	39.85	33.98	0.50
	28	36.31	16.30	27.78	30.66	0.55
	90	17.56	17.05	14.48	15.13	0.78
CC30LS15	7	40.48	24.65	27.23	34.46	0.46
	28	36.9	16.13	20.8	31.16	0.51
	90	25.99	13.97	15.42	17.69	0.75

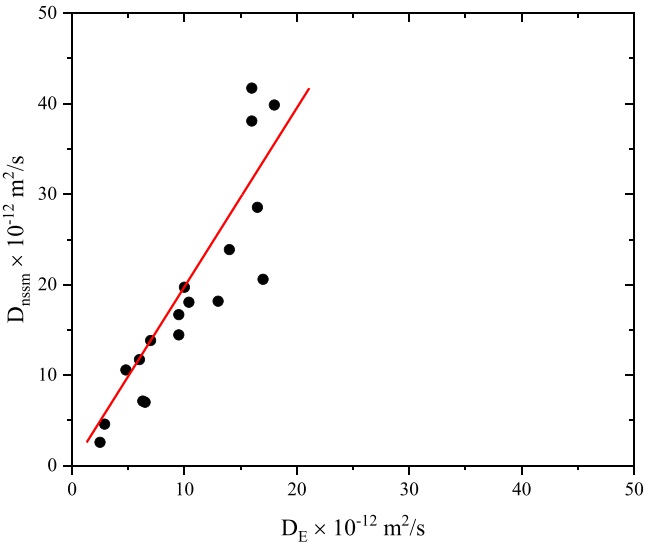

Fig. 11. Relation between chloride migration and diffusion.

chloride diffusion coefficient and the laboratory-measured values were used to evaluate the durability performance during the construction of Hong Kong–Zhuhai–Macau sea link project [46].

4.1.2. Relation between bulk conductivity / surface resistivity and chloride transport properties

The chloride migration process in cementitious system is mainly influenced by the potential drop across the specimen, meaning that the electrical conductivity and resistivity of mortar play a significant role. Fig. 12 shows the correlation of chloride transport coefficients with corresponding bulk conductivity and surface resistivity, taking into account values at 28 and 90 days of curing.

From the Figure it can be observed that the chloride migration coefficients are strongly influenced by the bulk conductivity and surface electrical resistivity of the mortar [47,48], which is less of a case with chloride diffusion coefficients. In a cementitious system, the electrical conductivity is mainly determined by the pore solution chemistry. The ion precipitation in the pore solution strongly varies with binder composition [49], and it is very difficult to decouple the effects of pore structure and resistivity of a cementitious system on chloride penetration [21].

4.1.3. Relation between sorptivity and chloride transport properties

Capillary absorption plays a significant role in the diffusion process, since one of the mechanisms of chloride transport is the convection. Because SCMs are present in binary and ternary mixtures, their sorptivity indices are lower. The addition of SCMs to the

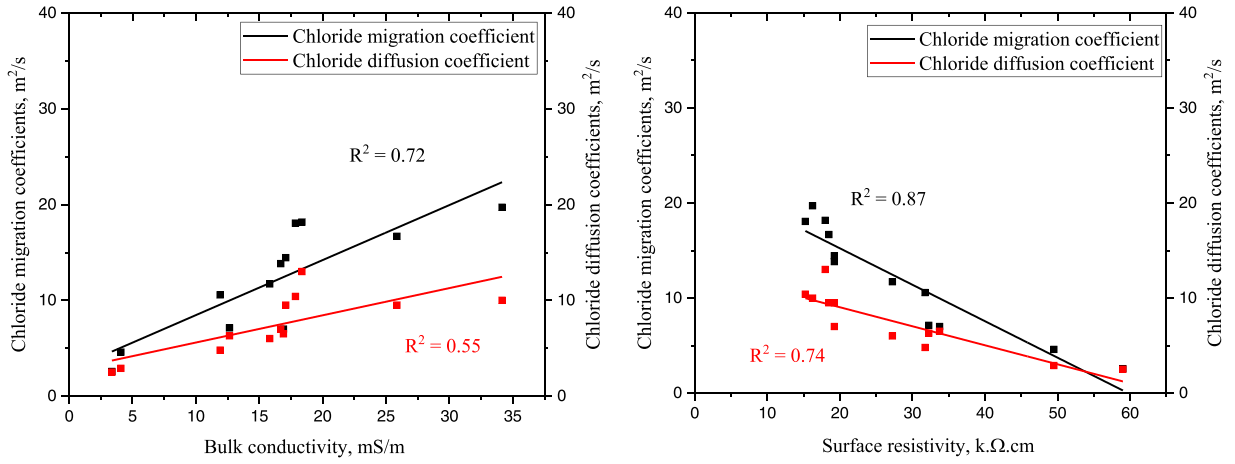

Fig. 12. Linear regression analysis of bulk conductivity and surface resistivity against chloride migration and diffusion coefficients.

system provided an additional pozzolanic and filler effect, resulting in a significant reduction in chloride absorption [50]. Furthermore, mortar with high sorptivity index would allow more chlorides to penetrate, especially in the surface layer of specimen. Fig. 13 shows the correlation between sorptivity indices and surface chloride content obtained after exposure of specimens according to NT BUILD 443 tests.

The correlation clearly shows that mortars with the higher sorptivity have a higher chloride intake from solution. Due to the capillary suction, concrete can immediately absorb the solution (containing chloride ions) from the environment, increasing the surface chloride concentration and therefore increasing chloride penetration [51]. However, chloride contents from other depths were not found to be correlated to the sorptivity index in the binary/ternary systems, rather to the physical and chemical characteristics of the binder.

4.2. Implication of pore structure on mortar properties

4.2.1. Compressive strength and pore structure

In general, increasing porosity reduces strength of cementitious materials, but the magnitude of this effect is dependent on pore size, shape, and distribution [52–55]. It was previously established that the strength of cement-based materials is directly proportional (1-permeable porosity(P)) and inversely proportional to square-root of median pore entry radius ($r_{0.5}$) [13,33,56]. Therefore, the relation can be written as:

$$\sigma = KC\frac{(1-P)}{\sqrt{r0.5}} \tag{8}$$

where K is the constant of proportionality and C is the cement content of the mix as fraction. The values of P and $r_{0.5}$ were determined using MIP curve and are given in Table 4. To determine the constant of proportionality, K, the experimental results of compressive strength were plotted against the corresponding $C(1\text{-}P)$/sqrt ($r_{0.5}$). Fig. 14 presents the relationship and the K value obtained was 260.15, with a coefficient of determination $R^2 = 0.98$.

4.2.2. Effect of permeable porosity and capillary porosity on chloride transport

There are several studies indicating a significant influence of the pore structure on the chloride transport mechanisms [57-59]. Among different types of pores, the penetration of chlorides is mainly attributed to the capillary pore size range [60]. The results of the total porosity accessible to mercury, i.e., permeable pore volume, indicate that the pore volume is decreased significantly after 90 days of curing. In blended system, the values of permeable porosity were higher than in CEM I at the early age because of the lower clinker amount, and consequently slower hydration reaction. CEM III samples also showed higher permeable porosity than CEM I but less than those observed for blended systems. The results show that after 90 days the porosity values decreased for fly ash and calcined clay mix, indicating that they start to alter the microstructure once the pozzolanic reaction occurs [6,60]. Fig. 15 shows the correlation between total permeable porosity and capillary pore volume with chloride migration and chloride diffusion coefficients.

The effective capillary pore volume is statistically more significantly correlated to transport phenomena in the tested systems, than the total permeable porosity. Furthermore, better correlation between pore parameters and transport parameters is obtained for diffusion than for migration coefficients. The volume of capillary pores decreases from 7 to 90 days due to the progress in hydration in all the mixtures. As expected, the 7-day value of capillary pore volume is very high, which is also reflected in the higher values of chloride transport coefficients. In the beginning of the hydration, the capillary pores are fully percolated and larger than C-S-H gel pores. Therefore, these capillary pores accelerate the chloride movement, thus higher values of chloride transport coefficients are obtained [61]. In the fly ash mix, the capillary pore volume has decreased around 60% from 7 days to 90 days and in the same period

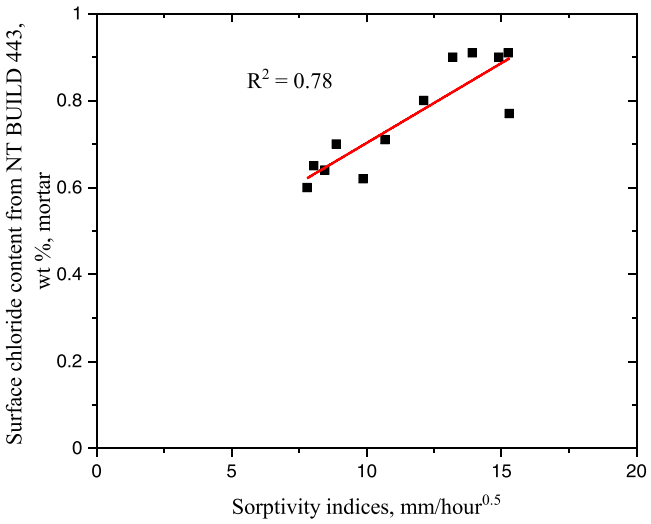

Fig. 13. Correlation between sorptivity indices and surface chloride content from NT BUILD 443.

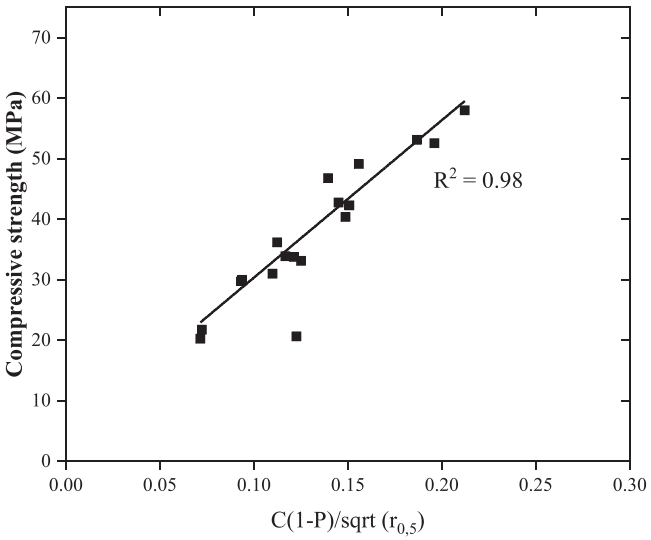

Fig. 14. Plot of compressive strength versus pore parameters C(1-P)/sqrt ($r_{0.5}$).

the chloride migration and diffusion coefficients decreased by around 70–73%. However, the capillary pore volumes of fly ash mix at both 7 and 28 days were higher than CEM I mix, while the chloride transport properties at 90 days were lower. The same trend was also observed for calcined clay mixture. In the case of CC30, capillary pores do not change significantly from 7 to 28 days, but after 28 days the pore volume was reduced for around 42%. When water-filled pores, obtained from sorptivity test, and capillary pores obtained from MIP, were compared (diagram not shown here), it was evident that the pore refinement due to the addition of SCMs mainly occurs in the capillary pore region, especially in the case of ternary blends [50]. Researchers have reported that in the early stage the calcined clay perform better than other SCMs, but in this study the lower content of kaolinite was responsible for lower clay reactivity [5]. However, the pore structure of calcined clay mix was continuously refined until 90 days, leading to the enhancement in the resistance to chlorides compared to CEM I. In CEM III, the values of the transport coefficients were the lowest, which was however not reflected in their porosity. More recent research [6] has shown that the low amount of kaolinite in clay mixtures influenced the capillary pore refinement, leading to less refinement than would be seen in a pure clay.

4.2.3. Effect of inter-connectivity of capillary pores on chloride transport

Inter connectivity of capillary pores plays significant role in chloride transport in cementitious system [62]. In SCM based binders, due to the pozzolanic reactions, the consumption of portlandite and formation of secondary C-S-H, inter-connectivity of pores is decreased with time which leads to a decrease in the chloride penetration [63]. There are different ways to show the degree of

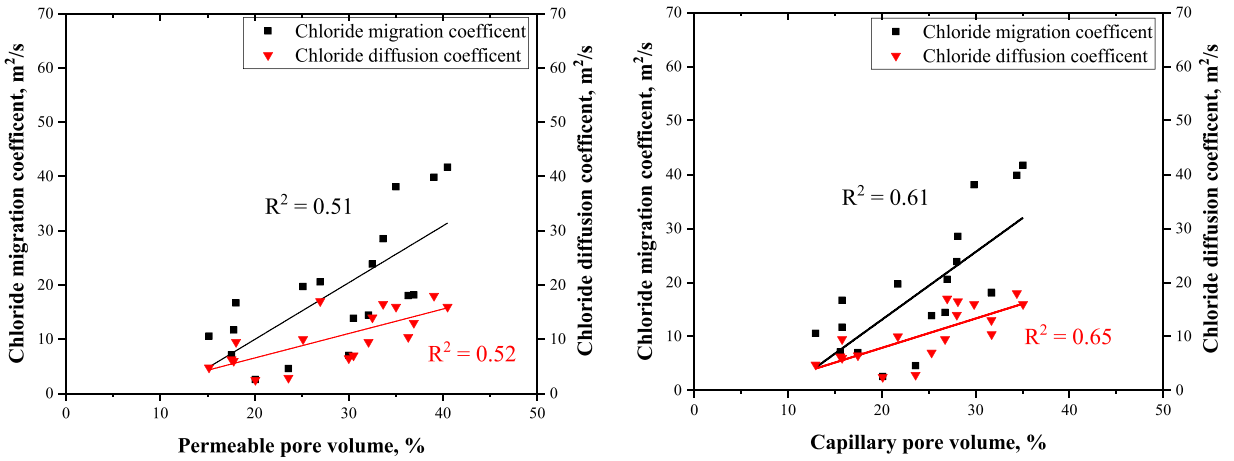

Fig. 15. Linear regression analysis of total permeable pore volume and capillary pore volume against chloride migration and diffusion coefficients.

inter-connectivity of the pore structure and the major parameters which can be drawn from MIP are critical pore radius and pore entrapment fraction. The values of critical pore entry radius and pore entrapment fraction are plotted against chloride migration and diffusion coefficients and illustrated in Fig. 16. Critical pore entry radius in MIP results implies the largest fraction of interconnected pores in a cementitious system. All the values of critical pore entry radius are reported in Table 4 and values were decreasing with prolonged curing. Similar to capillary pore volume, all the mixes showed high critical pore radius at 7 days, and then progressively lower values with hydration time. After 90 days, the lowest radius found was for fly ash mix FA30 and the highest for CEM I. Another parameter describing inter-connectivity is pore entrapment fraction. As seen in Table 4, the pore entrapment fraction increased with hydration progress. After 90 days of curing, both binary and ternary mixes showed better structure discontinuity in their pore structure, and that reflected their transport properties. Compared to pore entrapment fraction, critical pore entry radius would be better explanation of chloride transport in ternary mixes. In any case, ternary mix with fly ash and limestone exhibited the highest value of tortuosity and CEM I the lowest.

The evolution of migration and diffusion coefficient are increasing with critical entry radius. Yang C and Halamickova reported that the migration coefficients are directly proportional to the critical entry radius [10,57]. In this study, all samples showed a general tendency that higher critical pore radius produces higher chloride penetration. In general, the pozzolanic reaction from fly ash and calcined clay can offset the dilution effect by filling the interim space between with C-A-S-H, continuing to progressively contribute and accelerate pore diameter reduction [64]. It is therefore that the values of critical pore entry radius were found to be lower in fly ash and clay mixes, compared to CEM I after 90 days. Pore entrapment fraction and chloride transport coefficients were also subjected to regression analysis, with the correlation found to be weaker than for other pore structure parameters. This could be due to the direct determination of pore connectivity values, particularly due to mixture heterogeneity in cementitious system. CEM III samples had the highest resistance to chloride penetration of all tested mixes, but the pore structure could not be improved enough to achieve this trend.

In terms of compressive strength and chloride diffusion coefficient, the low-grade kaolin clay mixtures performed similarly to CEM I

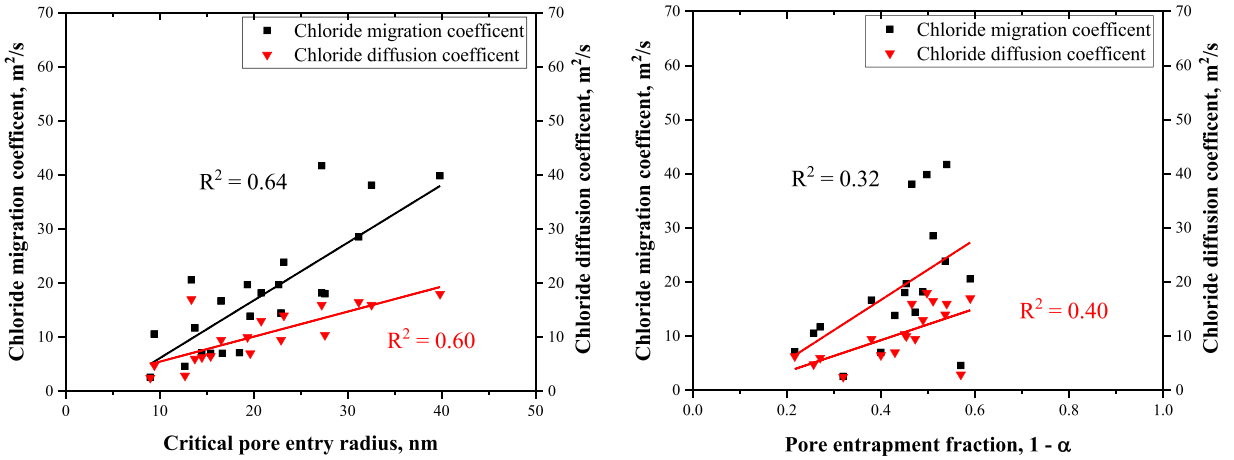

Fig. 16. Linear regression analysis of critical pore entry radius and pore entrapment fraction against chloride transport coefficients.

and CEM III. The pore structure parameters of the calcined clay mixture were refined after 90 days of curing, and the refinement contributed to the resistance to ion movement, as shown by the chloride migration results. The chloride migration coefficients showed a weaker linear dependence on the pore structure parameters compared to the diffusion coefficient. The reason could be that the migration coefficients are strongly influenced by the conducting ions in the pore solution [48]. Therefore, all pore structure parameters have a limited effect on chloride penetration in blended cementitious systems, indicating that other parameters of blended systems, such as chloride binding capacity could have a prevailing role [10,15,65,66]. The binding of chloride ions in various hydrates, particularly C-A-S-H and AFm phases, retards chloride penetration in cementitious systems. In the systems based on limestone-calcined clay, the amount of carbo-aluminate hydrate increases as kaolinite content rises. Therefore, the effective binding capacity might be advantageous for kaolinite-rich clays [5,6]. Maraghechi et al. [6] measured the apparent diffusion coefficient of a cementitious system with different amounts of kaolinite, from 17% to 95%. They found that the chloride diffusion was greatly reduced as the amount of kaolinite increased. However, when the kaolinite content went from 50% to 95%, the effect on the chloride ingress resistance was less significant. Due to the high level of replacement, the amount of portlandite available for clay is limited, preventing formation of additional hydration products. Therefore, the optimal would be that all of the portlandite is used up in the reaction with calcined clay and limestone, leaving no unreacted metakaolin behind [7]. Present study confirms that even clays with a lower amount of kaolin, such as those in mixes CC30 and CC30LS15, can be used to prepare concrete with good resistance to chloride ingress.

5. Conclusion

This paper put forward insights on how the mechanical and chloride penetration resistance change with the substitution of cement with a low-kaolin clay. Furthermore, study analysed the impact of different durability parameters, such as sorptivity and surface electrical resitivity, and pore structure parameters, on chloride transport in blended systems. Pore structure parameters that were analysed include capillary porosity, critical pore entry radius, mean entry radius, and pore entrapment fraction.

The ternary mixes with the addition of limestone prepared and tested in this study had similar durability to the binary mixes and were better than Portland cement. However, their mechanical properties were significantly lower compared to the CEM I mortar. The chloride migration coefficients of blended mixes were strongly influenced by the electrical conductivity and surface resistivity of the system. This influence was stronger in the case of chloride migration coefficients than chloride diffusion coefficients. Chloride migration coefficients were significantly higher (1.86 times) than diffusion coefficients. The over-estimation in chloride migration coefficients should be taken into account when using values of rapid chloride migration test in the estimation of service life of blended mixes.

Regardless of the MIP constraint, the results showed an acceptable correlation between certain pore structure parameters, such as permeable and capillary pore volume, critical pore radius and pore entrapment fraction, and the chloride transport coefficient. The critical pore radius and capillary pore volume showed a stronger influence on chloride penetration than other parameters. Moreover, the correlation of pore structure parameters was relatively stronger with chloride diffusion than with chloride migration coefficients. Regardless, pore structure parameters cannot be used to fully explain chloride ingress in blended cementitious systems. This study highlights the importance of revealing the chloride interaction due to the binding effect of the C-S-H surface and the effects of the charged C-S-H surface to fully understand chloride ingress in these systems.

All of the alternative cementitious materials used in this study were locally available. Despite the relatively low kaolinite content, the calcined clay used in the study performed better than ordinary Portland cement mortar in terms of chloride penetration and showed comparable results to slag cement. Thus, even low-grade, locally available clays can be a good choice for cementitious materials with good resistance to chloride penetration and low CO_2 content.

Declaration of Competing Interest

The authors declare that they have no known competing financial interests or personal relationships that could have appeared to influence the work reported in this paper.

Data availability

Data will be made available on request.

Acknowledgment

The presented research is a part of a scientific project “Advanced low CO_2 cementitious materials”, ACT (grant no. IZHRZO 180590/1), financed within the Croatian–Swiss Research Program of the Croatian Science Foundation and the Swiss National Science Foundation with funds obtained from the Swiss-Croatian Cooperation Program. The first two authors also acknowledge the support of the project “Alternative binders for concrete: understanding microstructure to predict durability”, ABC (grant no. HRZZ-UIP-2017–05-4767), financed by Croatian Science Foundation.

References

[1] K.L. Scrivener, V.M. John, E.M. Gartner, Eco-efficient cements: Potential economically viable solutions for a low-CO_2 cement-based materials industry, Cem. Concr. Res. vol. 114 (2018) 2–26, https://doi.org/10.1016/j.cemconres.2018.03.015.
[2] K. Scrivener, F. Martirena, S. Bishnoi, S. Maity, Calcined clay limestone cements (LC3), Cem. Concr. Res. vol. 114 (2018) 49–56, https://doi.org/10.1016/j.cemconres.2017.08.017.
[3] H. Du, S.D. Pang, High-performance concrete incorporating calcined kaolin clay and limestone as cement substitute, Constr. Build. Mater. vol. 264 (. 2020), 120152, https://doi.org/10.1016/j.conbuildmat.2020.120152.
[4] R. Fernandez, F. Martirena, K.L. Scrivener, Cement and Concrete Research The origin of the pozzolanic activity of calcined clay minerals: A comparison between kaolinite, illite and montmorillonite, Cem. Concr. Res. vol. 41 (1) (2011) 113–122, https://doi.org/10.1016/j.cemconres.2010.09.013.
[5] F. Avet, K. Scrivener, Investigation of the calcined kaolinite content on the hydration of Limestone Calcined Clay Cement (LC3), Cem. Concr. Res. vol. 107 (2018) 124–135, https://doi.org/10.1016/j.cemconres.2018.02.016.
[6] H. Maraghechi, F. Avet, H. Wong, H. Kamyab, K. Scrivener, Performance of Limestone Calcined Clay Cement (LC3) with various kaolinite contents with respect to chloride transport, Mater. Struct. Constr. vol. 51 (5) (2018) 1–17, https://doi.org/10.1617/s11527-018-1255-3.
[7] Krishnan, S., Gopala Rao, D., and Bishnoi, S., Why Low-Grade Calcined Clays Are the Ideal for the Production of Limestone Calcined Clay Cement (LC3) BT - Calcined Clays for Sustainable Concrete, 2020, pp. 125–130.
[8] A. Zolfagharnasab, A.A. Ramezanianpour, F. Bahman-zadeh, Investigating the potential of low-grade calcined clays to produce durable LC 3 binders against chloride ions attack, Constr. Build. Mater. vol. 303 (2021), 124541, https://doi.org/10.1016/j.conbuildmat.2021.124541.
[9] M. Frías, J. Cabrera, Pore size distribution and degree of hydration of metakaolin-cement pastes, Cem. Concr. Res. vol. 30 (4) (2000) 561–569, https://doi.org/10.1016/S0008-8846(00)00203-9.
[10] P. Halamickova', R.J. Detwiler, D.P. Bentz3, E.J. Garbocz, Permeability and chloride diiffusion, Cem. Concr. Res. vol. 25 (4) (1995) 790–802.
[11] S. Diamond, Mercury porosimetry. An inappropriate method for the measurement of pore size distributions in cement-based materials, Cem. Concr. Res. vol. 30 (10) (2000) 1517–1525, https://doi.org/10.1016/S0008-8846(00)00370-7.
[12] K.L. Willis, A.B. Abell, D.A. Lange, Image-based characterization of cement pore structure using Wood's metal intrusion, Cem. Concr. Res. vol. 28 (12) (1998) 1695–1705, https://doi.org/10.1016/S0008-8846(98)00159-8.
[13] B.B. Das, B. Kondraivendhan, Implication of pore size distribution parameters on compressive strength, permeability and hydraulic diffusivity of concrete, Constr. Build. Mater. vol. 28 (1) (2012) 382–386, https://doi.org/10.1016/j.conbuildmat.2011.08.055.
[14] B. Bhattacharjee, S. Krishnamoorthy, Permeable Porosity and Thermal Conductivity of Construction Materials, J. Mater. Civ. Eng. vol. 16 (4) (2004) 322–330, https://doi.org/10.1061/(asce)0899-1561(2004)16:4(322).
[15] S. Sui, F. Georget, H. Maraghechi, W. Sun, K. Scrivener, Towards a generic approach to durability: Factors affecting chloride transport in binary and ternary cementitious materials, Cem. Concr. Res. vol. 124 (2019), 105783, https://doi.org/10.1016/j.cemconres.2019.105783.
[16] Monfore, G.E., The electrical resistivity of concrete, 1968.
[17] B.B. Hope, A.K. Ip, D.G. Manning, Corrosion and electrical impedance in concrete, Cem. Concr. Res. vol. 15 (3) (1985) 525–534.
[18] H.W. Whittington, J. McCarter, M.C. Forde, The conduction of electricity through concrete, Mag. Concr. Res. vol. 33 (114) (1981) 48–60.
[19] H. Layssi, P. Ghods, Alizadeh, R. Aali, M. Salehi, Electrical resistivity of concrete, Concr. Int., no. (2016) 41–46.
[20] S. Feliu, C. Andrade, J.A. González, C. Alonso, A new method forin-situ measurement of electrical resistivity of reinforced concrete, Mater. Struct. vol. 29 (6) (1996) 362–365.
[21] C. Shi, Q. Yuan, F. He, X. Hu, Transport and Interactions of Chlorides in Cement-based Materials, CRC Press,, 2019.
[22] M. Flegar, M. Serdar, D. Londono-Zuluaga, K. Scrivener, Regional waste streams as potential raw materials for immediate implementation in cement production, Mater. (Basel) vol. 13 (23) (2020) 1–15, https://doi.org/10.3390/ma13235456.
[23] K. Scrivener, R. Snellings, B. Lothenbach, A Practical Guide to Microstructural Analysis of Cementitious Materials, vol. 540, Crc Press,, Boca Raton, FL, USA, 2016.
[24] K. Scrivener, F. Avet, H. Maraghechi, F. Zunino, J. Ston, W. Hanpongpun, A. Favier, Impacting factors and properties of limestone calcined clay cements (LC3), Green. Mater. vol. 7 (1) (2018) 3–14, https://doi.org/10.1680/jgrma.18.00029.
[25] 196–10:2016, B. E., BSI Standards Publication Methods of testing cement, no. Vi, 2016.
[26] N.T. Build, 492, Concrete, mortar and cement-based repair materials: Chloride migration coefficient from non-steady-state migration experiments, Measurement (1999) 1–8.
[27] A.V. Lebedev, The synthesis of multi-channel adaptive control system for the autonomous underwater robot, RPC 2010 - 1st Russ. Pac. Conf. Comput. Technol. Appl. (2010) 324–328.
[28] BSI, BS EN 14629:2007 Products and systems for the protection and repair of concrete structures - Test methods - Determination of chloride content in hardened concrete, vol. 3, 2007.
[29] Test, C.C., Cabinets, M., Rooms, M., Test, C.C., Drilled, T., and Ag-, C., Standard Test Method for Bulk Electrical Conductivity of Hardened Concrete 1, pp. 4–7, 2013, doi: ⟨10.1520/C1760–12.2⟩.
[30] F.M. FDOT, FM 5-578: Florida method of test for concrete resistivity as an electrical indicator of its permeability, Fla. Dep. Transp. (2004).
[31] M. Alexander, Y. Ballim, J.M. Mackechnie, Durability index testing procedure manual, Res. Monogr. vol. 2018 (No.4) (2018) 29.
[32] S. Diamond, Mercury porosimetry: an inappropriate method for the measurement of pore size distributions in cement-based materials, Cem. Concr. Res. vol. 30 (10) (2000) 1517–1525.
[33] R. Kumar, B. Bhattacharjee, Porosity, pore size distribution and in situ strength of concrete, Cem. Concr. Res. vol. 33 (1) (2003) 155–164, https://doi.org/10.1016/S0008-8846(02)00942-0.
[34] F. Moro, H. Böhni, Ink-bottle effect in mercury intrusion porosimetry of cement-based materials, J. Colloid Interface Sci. vol. 246 (1) (2002) 135–149, https://doi.org/10.1006/jcis.2001.7962.
[35] N. Nair, K. Mohammed Haneefa, M. Santhanam, R. Gettu, A study on fresh properties of limestone calcined clay blended cementitious systems, Constr. Build. Mater. vol. 254 (2020), 119326, https://doi.org/10.1016/j.conbuildmat.2020.119326.
[36] H.-J. Chen, N.-H. Shih, C.-H. Wu, S.-K. Lin, Effects of the loss on ignition of fly ash on the properties of high-volume fly ash concrete, Sustainability vol. 11 (9) (2019) 2704.
[37] K. De Weerdt, M. Haha, Ben, G. Le Saout, K.O. Kjellsen, H. Justnes, B. Lothenbach, Hydration mechanisms of ternary Portland cements containing limestone powder and fly ash, Cem. Concr. Res. vol. 41 (3) (2011) 279–291, https://doi.org/10.1016/j.cemconres.2010.11.014.
[38] M. Antoni, J. Rossen, F. Martirena, K. Scrivener, Cement substitution by a combination of metakaolin and limestone, Cem. Concr. Res. vol. 42 (12) (2012) 1579–1589, https://doi.org/10.1016/j.cemconres.2012.09.006.
[39] S. Antiohos, S. Tsimas, Investigating the role of reactive silica in the hydration mechanisms of high-calcium fly ash/cement systems, Cem. Concr. Compos. vol. 27 (2) (2005) 171–181, https://doi.org/10.1016/j.cemconcomp.2004.02.004.
[40] A.A. Ramezanianpour, A. Pilvar, M. Mahdikhani, F. Moodi, Practical evaluation of relationship between concrete resistivity, water penetration, rapid chloride penetration and compressive strength, Constr. Build. Mater. vol. 25 (5) (2011) 2472–2479, https://doi.org/10.1016/j.conbuildmat.2010.11.069.
[41] J. Wang, E. Liu, The relationship between steady-state chloride diffusion and migration coefficients in cementitious materials, Mag. Concr. Res. vol. 72 (19) (2020) 1016–1026.
[42] Y. Dhandapani, M. Santhanam, Assessment of pore structure evolution in the limestone calcined clay cementitious system and its implications for performance, Cem. Concr. Compos. vol. 84 (2017) 36–47, https://doi.org/10.1016/j.cemconcomp.2017.08.012.
[43] M.G. Alexander, J.R. Mackechnie, Y. Ballim, Guide to the use of durability indexes for achieving durability in concrete structures, Res. Monogr. vol. 2 (1999) 102.

[44] M. Castellote, C. Andrade, Round-Robin test on methods for determining chloride transport parameters in concrete, Mater. Struct. Constr. vol. 39 (294) (2006) 955–990, https://doi.org/10.1617/s11527-006-9193-x.
[45] Yuan, Q., Fundamental Studies on Test Methods for the Transport ofChloride Ions in Cementitious Materials. Ghent University, 2009.
[46] K. Li, Q. Li, X. Zhou, Z. Fan, Durability design of the Hong Kong–Zhuhai–Macau sea-link project: principle and procedure, J. Bridg. Eng. vol. 20 (11) (2015), 04015001, https://doi.org/10.1061/(asce)be.1943-5592.0000741.
[47] P. Gao, J. Wei, T. Zhang, J. Hu, Q. Yu, Modification of chloride diffusion coefficient of concrete based on the electrical conductivity of pore solution, Constr. Build. Mater. vol. 145 (2017) 361–366, https://doi.org/10.1016/j.conbuildmat.2017.03.220.
[48] C. Shi, Effect of mixing proportions of concrete on its electrical conductivity and the rapid chloride permeability test (ASTM C1202 or ASSHTO T277) results, Cem. Concr. Res. vol. 34 (3) (2004) 537–545, https://doi.org/10.1016/j.cemconres.2003.09.007.
[49] M. Thomas, The effect of supplementary cementing materials on alkali-silica reaction: A review, Cem. Concr. Res. vol. 41 (12) (2011) 1224–1231, https://doi.org/10.1016/j.cemconres.2010.11.003.
[50] Y. Dhandapani, T. Sakthivel, M. Santhanam, R. Gettu, R.G. Pillai, Mechanical properties and durability performance of concretes with Limestone Calcined Clay Cement (LC3), Cem. Concr. Res. vol. 107 (2018) 136–151, https://doi.org/10.1016/j.cemconres.2018.02.005.
[51] D. Conciatori, H. Sadouki, E. Brühwiler, Capillary suction and diffusion model for chloride ingress into concrete, Cem. Concr. Res. vol. 38 (12) (2008) 1401–1408, https://doi.org/10.1016/j.cemconres.2008.06.006.
[52] Popovics, S., New formulas for the prediction of the effect of porosity on concrete strength, in *Journal Proceedings*, 1985, vol. 82, no. 2, pp. 136–146.
[53] C. Shi, Strength, pore structure and permeability of alkali-activated slag mortars, Cem. Concr. Res. vol. 26 (12) (1996) 1789–1799.
[54] M. O'Farrell, S. Wild, B.B. Sabir, Pore size distribution and compressive strength of waste clay brick mortar, Cem. Concr. Compos. vol. 23 (1) (2001) 81–91.
[55] C.E. Wen, Y. Yamada, K. Shimojima, Y. Chino, H. Hosokawa, M. Mabuchi, Compressibility of porous magnesium foam: dependency on porosity and pore size, Mater. Lett. vol. 58 (3–4) (2004) 357–360.
[56] Atzeni, C., Effect of pore distribution on strength of hardened cement pastes, in *Pore Structure and Materials Properties, Proceedings of the First International RILEM Congress*, 1987, vol. 1, pp. 195–202.
[57] C.-C. Yang, On the relationship between pore structure and chloride diffusivity from accelerated chloride migration test in cement-based materials, Cem. Concr. Res. vol. 36 (7) (2006) 1304–1311.
[58] C.-C. Yang, S.W. Cho, L.C. Wang, The relationship between pore structure and chloride diffusivity from ponding test in cement-based materials, Mater. Chem. Phys. vol. 100 (2–3) (2006) 203–210.
[59] E.J. Garboczi, D.P. Bentz, Computer simulation of the diffusivity of cement-based materials, J. Mater. Sci. vol. 27 (8) (1992) 2083–2092.
[60] C. Li, L. Jiang, N. Xu, S. Jiang, Pore structure and permeability of concrete with high volume of limestone powder addition, Powder Technol. vol. 338 (2018) 416–424, https://doi.org/10.1016/j.powtec.2018.07.054.
[61] C.C. Yang, S.W. Cho, L.C. Wang, The relationship between pore structure and chloride diffusivity from ponding test in cement-based materials, Mater. Chem. Phys. vol. 100 (2–3) (2006) 203–210, https://doi.org/10.1016/j.matchemphys.2005.12.032.
[62] Y. Dhandapani, M. Santhanam, Investigation on the microstructure-related characteristics to elucidate performance of composite cement with limestone-calcined clay combination, Cem. Concr. Res. vol. 129 (2020), 105959, https://doi.org/10.1016/j.cemconres.2019.105959.
[63] G.K. Glass, N.R. Buenfeld, Chloride-induced corrosion of steel, Prog. Struct. Eng. Mater. vol. 2 (4) (2000) 448–458.
[64] J.H. Filho, M.H.F. Medeiros, E. Pereira, P. Helene, G.C. Isaia, High-volume fly ash concrete with and without hydrated lime: chloride diffusion coefficient from accelerated test, J. Mater. Civ. Eng. vol. 25 (3) (2013) 411–418, https://doi.org/10.1061/(asce)mt.1943-5533.0000596.
[65] K. Wu, H. Shi, L. Xu, G. Ye, G. De Schutter, Microstructural characterization of ITZ in blended cement concretes and its relation to transport properties, Cem. Concr. Res. vol. 79 (2016) 243–256, https://doi.org/10.1016/j.cemconres.2015.09.018.
[66] Q. Yuan, C. Shi, G. De Schutter, K. Audenaert, D. Deng, Chloride binding of cement-based materials subjected to external chloride environment - A review, Constr. Build. Mater. vol. 23 (1) (2009) 1–13, https://doi.org/10.1016/j.conbuildmat.2008.02.004.